

Transport properties of high- T_c $\text{Bi}_2\text{Sr}_2\text{CaCu}_2\text{O}_{8+\delta}$ crystals near the superconducting transition

Y. M. Wan

Department of Physics, National Tsing Hua University, Hsinchu, Taiwan 300, Republic of China

T. R. Lemberger, S. E. Hebboul, and J. C. Garland

Department of Physics, Ohio State University, Columbus, Ohio 43210

(Received 29 January 1996)

We report a multiterminal experiment on BSCCO single crystals in zero magnetic field to study the transport properties from transition to room temperature. In the normal state, analysis of using a linear resistivity model suggests that the system is linear. In transition, current-voltage characteristics of the ab plane, of the c axis, and of the secondary layer using a flux transformer method show nonlinearity. All these nonlinear features can be put into a self-consistent scheme within the context of in-plane thermal excitation of vortices, and an out-of-plane Josephson interaction. [S0163-1829(96)01829-2]

I. INTRODUCTION

The intrinsic layered structure of high- T_c oxides have been known to give rise to many interesting and unconventional phenomena over a broad temperature range. In the normal state, the most astonishing feature is the dramatically different temperature dependence of the in-plane and out-of-plane resistivity along with an anisotropy ratio ranging from 10^5 to 10^3 . In transition without the presence of an external magnetic field on the highly conducting CuO_2 bilayers, Kosterlitz-Thouless¹ resistive transition has been observed with evidence found in the square-root temperature dependence of in-plane resistivity,² in the nonlinear current voltage characteristics,³ and in the magnetic screening of vortices in a magnetic field.²

In corroboration with the interlayer Josephson interaction,⁴ three-dimensional thermal vortices, which are pictured as aligned two-dimensional (2D) vortices, were proposed⁵ and examined experimentally in a fixed point in magnetization curves. An interesting transport result associated with the interlayer coupling scheme reported more recently is the observation of the secondary voltage peaks in the measurements of using the dc flux transformer geometry by the authors,⁶ in which a constant current is applied to the primary layer with voltage recorded on the secondary layer. Similar to the dc-flux transformer study, lately, the correlated magnetic noise due to the motion of thermal vortices from the top to the bottom surfaces has also been detected by using two SQUID's.⁷

Parallel to these experimental works, there are progressive achievements in the study of the transport nature. As guided by the observation of the secondary peaks, Horowitz⁸ argued that these peaks are a manifestation of the interaction of intralayer vortices and interlayer fluxons. Focusing on the interlayer correlation length of vortices in a vortex gas model in which two-body interactions are considered, Pierson⁹ interpreted the peaks as vortex loops unbinding and layer decoupling. Using a two-layer Josephson junction array, Yu and Stroud¹⁰ concluded that the pronounced secondary peaks can be a result of the interlayer Josephson interaction only without invoking magnetic interaction. By changing the ratio

of the out-of-plane coupling strength to the in plane, Uprety and Domínguez¹¹ have simulated the current-voltage characteristics on the secondary layer, comparable to experimental results.

Regardless of so many studies, questions still remain and there is also a lack of comprehensive exploration of the transport nature across the superconducting transition. To clarify this issue, in this work we perform throughout transport measurements on BSCCO(2212) single crystals in the temperature regime from ~ 85 to 300 K. We find that this material is linear above T_c and can be well understood on a 3D linear anisotropic resistivity (3LAR) model. Furthermore our study shows that the current-voltage characteristics taken from over all the surfaces can be put into a unified picture in terms of thermally created layer vortices and interlayer coupling.

Three single crystals with a transition near ~ 85 K were prepared by a solid-state reaction method. In brief, an appropriate amount of Bi_2O_3 , CuO , CaCO_3 , and SrCO_3 oxide powders was uniformly mixed and grounded. Then this mixture was loaded in a gold crucible and heated in dry oxygen gas. The temperature of the oven was ramped within a couple of hours to 920°C at which the temperature was held for 5 h before the cooling process. The initial cooling was at a very slow rate 1°C/h to 820°C , then at an intermediate rate of $\sim 100^\circ\text{C/h}$ to 400°C , and finally furnace cooled by turning off the oven. Single crystals were taken out of the crucible mechanically. The typical sizes were a millimeter in the ab plane and $\sim 20\ \mu\text{m}$ thick along the c axis. These selected crystals were postannealed in oxygen atmosphere for more than 24 h at $500\text{--}600^\circ\text{C}$ to improve the oxygen homogeneity. One side polished ($1\ \text{mm}\times 1\ \text{mm}\times 0.5\ \text{mm}$) MgO crystals were used to mount sample and electrical contacts. As shown in Fig. 1(a), up to six electrical contacts were attached to a sample. Silver adhesive (ACME 3022) and gold wires were used to implement the electrical contacts. Contact resistance less than $5\ \Omega$ was achieved by firing at $400\text{--}500^\circ\text{C}$ for 1–2 h without a noticeable degrade of sample quality.

Our measurements were performed inside a variable-temperature cryostat immersed in a ^4He bath. To perform a

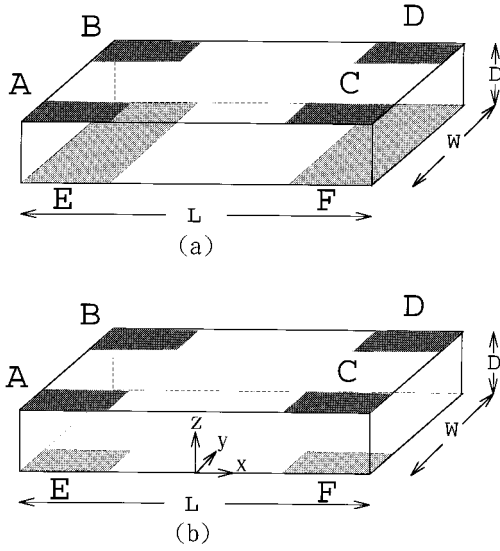


FIG. 1. Multiple-terminal configurations of our measurements. (a) Six electrical contacts for sample A where four contacts of size $L/4 \times W/4$ are on the primary layer and two of $L/4 \times W$ on the secondary layer. (b) The modified contact geometry for the 3LAR model analysis, the bottom contacts are reduced to $L/4 \times W/4$. The origin of the Cartesian coordinate shown here is for the ab -plane analysis, while for the c -axis analysis, the center is at the left end corner on the contact E.

zero-field study, the cryostat was screened by superconducting Pb foils, with a residual internal field less than 20 mG. Sample temperature was monitored with a carbon glass thermometer over the temperature range 4–300 K. Current-voltage and resistive measurements were made using a four-terminal technique in which square wave currents (16.9 Hz) were applied by a current source and the sample voltages detected with a lock-in amplifier. With the six electrical contacts [Fig. 1(a)], we managed to perform three types of measurements. On the ab plane the current was through contacts A and C, voltage V_{ab} monitored across B and D. Along the c axis the current was applied through contacts A and E and voltage V_c recorded across C and F. For the dc-flux transformer geometry, we used the contacts A and C as current leads and E and F for voltage V_s .

II. 3D LINEAR ANISOTROPIC RESISTIVITY MODEL

To analyze our data, we developed a three-dimensional linear resistivity (3LAR) model specifically for our measurements. One shall see that this model can be readily modified for similar multiterminal measurements. The starting point is the conservation law of current, namely, the Laplace equation as shown in Eq. (1) in which J and V represent the

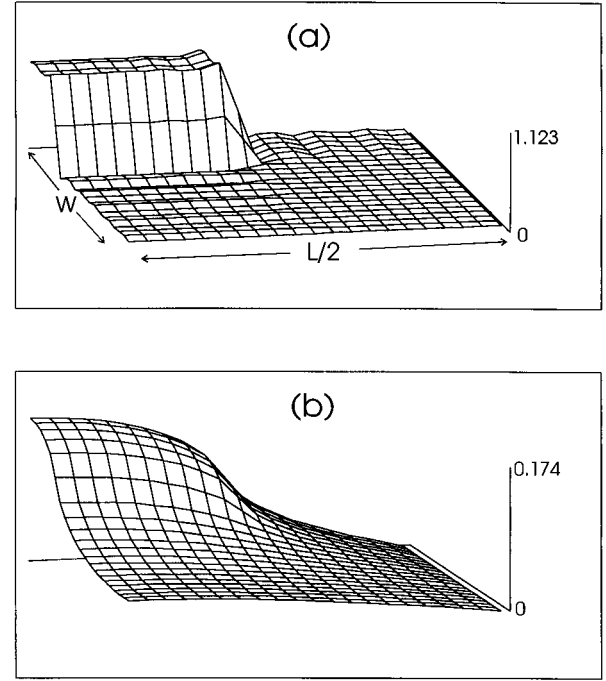


FIG. 2. Linear resistivity model simulations for (a) normalized current density and (b) the electrical potential on the primary layer of a crystal in the ab -plane measurements.

electrical current density and electrical potential in the sample, while ρ_a , ρ_b , and ρ_c denote the principle resistivity along the crystalline a , b , and c axes. Since the resistivity along the a and b axes is known to be approximately equal (within a factor of 2), we can simplify Eq. (1) by replacing ρ_a and ρ_b with $\rho_{ab} = (\rho_a \rho_b)^{1/2}$ and have Eq. (2):

$$\nabla \cdot J = \frac{1}{\rho_a} \frac{\partial^2 V}{\partial^2 x} + \frac{1}{\rho_b} \frac{\partial^2 V}{\partial^2 y} + \frac{1}{\rho_c} \frac{\partial^2 V}{\partial^2 z} = 0, \quad (1)$$

$$\nabla \cdot J = \frac{1}{\rho_{ab}} \frac{\partial^2 V}{\partial^2 x} + \frac{1}{\rho_{ab}} \frac{\partial^2 V}{\partial^2 y} + \frac{1}{\rho_c} \frac{\partial^2 V}{\partial^2 z} = 0. \quad (2)$$

The solution for Eq. (2) is better expressed in a Fourier series to cooperate with the rectangular sample geometry. In the following, we will correlate the experimental parameters V_{ab} , V_s , and V_c to the crystalline resistivity ρ_{ab} and ρ_c in two cases.

A. ab -plane measurements

For these measurements, we formulate the series solution as Eq. (3) by setting the origin of the Cartesian coordinate at the center of the bottom layer as illustrated in Fig. 1(b),

$$V = \sum_{n,m} V_{nm} \sin\left(\frac{n\pi x}{L}\right) \cos\left(\frac{m\pi y}{W}\right) \cosh\left[\pi \sqrt{\left(\frac{\rho_c}{\rho_{ab}}\right)} \sqrt{\left(\frac{n}{L}\right)^2 + \left(\frac{m}{W}\right)^2} z\right], \quad (3)$$

where L stands for the sample length, W for the width. M are integers ≥ 0 ; and n are odd integers > 0 . Since the applied current flows in and out the sample via the primary layer, there is no current coming out of the rest surfaces. In other words,

the normal component of electrical field should be zero. In fact it is true that the normal components of electrical fields at the surfaces of $x = \pm L/2$, $y=0$ are zero. With the orthogonal properties of sin and cos functions, the coefficient V_{nm} in the series can be determined by the following double integration over the primary layer:

$$\int_{-L/2}^{L/2} \int_0^W \sin\left(\frac{n\pi x}{L}\right) \cos\left(\frac{m\pi y}{W}\right) J(x,y,z) dx dy = - \int_{-L/2}^{L/2} \sin\left(\frac{n\pi x}{L}\right) dx \int_0^W dy \cos\left(\frac{m\pi y}{W}\right) \frac{1}{\rho_c} \frac{\partial V}{\partial z}. \quad (4)$$

On the left-hand side of the equation, the area contributing to the integration is on the current pads (from 0 to $W/4$ and 0 to $L/4$) on which the current density is assumed to be uniform, i.e., $J = 16I/LW$. Whereas on the right-hand side, the contribution is from all over the surface. Assuming $n > 0$ and $m = 0$, we have

$$V_{n0} = \frac{16Ik \cos(n\pi/4) \sin(m\pi/4)}{nmLW\pi^3 \sinh(pn\pi D/L)}, \quad (5)$$

where k is the abbreviation for $(\rho_c \rho_{ab})^{1/2}$ and p is for $(\rho_c/\rho_{ab})^{1/2}$. For $n > 0$ and $m > 0$, we find

$$V_{nm} = \frac{128Ik \cos(n\pi/4) \sin(m\pi/4)}{nmLW\pi^3 \sqrt{[(n/L)^2 + (m/W)^2]} \sinh\{p\pi \sqrt{[(n/L)^2 + (m/W)^2]} D\}}. \quad (6)$$

By plugging these coefficients into Eq. (3), we calculate the potential difference between points $(x,y,z=D)$ and $(-x,y,z=D)$ on the primary plane and the result is

$$V_{ab}(x,y) = \frac{32Ik}{W} \sum_{n=1}^{\infty} \frac{\cos(n\pi/4) \sin(n\pi x/L)}{n^2 \pi^2 \tanh[pn\pi(D/L)]} + \frac{256Ik}{W} \sum_{n=1}^{\infty} \sum_{m=1}^{\infty} \frac{\cos(n\pi/4) \sin(n\pi x/L) \sin(m\pi/4) \cos(m\pi y/W)}{nm\pi^3 \sqrt{n^2 + (mL/W)^2} \tanh[p\pi \sqrt{n^2 + (mL/W)^2} (D/L)]}. \quad (7)$$

On the secondary layer the potential difference between points $(x,y,z=0)$ and $(-x,y,z=0)$ can be obtained as

$$V_s(x,y) = \frac{32Ik}{W} \sum_{n=1}^{\infty} \frac{\cos(n\pi/4) \sin(n\pi x/L)}{n^2 \pi^2 \sinh[pn\pi(D/L)]} + \frac{256Ik}{W} \sum_{n=1}^{\infty} \sum_{m=1}^{\infty} \frac{\cos(n\pi/4) \sin(n\pi x/L) \sin(m\pi/4) \cos(m\pi y/W)}{nm\pi^3 \sqrt{n^2 + (mL/W)^2} \sinh[p\pi \sqrt{n^2 + (mL/W)^2} (D/L)]}. \quad (8)$$

We check the validity of the all the calculations by computing the normalized current density of Eq. (9) and that is expect to reproduce the exact experimental condition

$$\frac{J/16I}{LW} = \sum_{n=1}^{\infty} \frac{\cos(n\pi/4) \sin(n\pi x/L)}{n\pi} + \sum_{n=1}^{\infty} \sum_{m=1}^{\infty} \frac{8 \cos(n\pi/4) \sin(m\pi/4) \sin(n\pi x/L) \cos(m\pi y/W)}{nm\pi^2}. \quad (9)$$

As shown in Fig. 2(a), with n and m up to 25, we find that the value of the normalized current density is unity on the current contact and zero elsewhere satisfying the experimental condition.

B. c -axis measurements

For the c -axis measurement, by using the same methodology as above we construct a somewhat more complicated series solution as Eq. (10),

$$V(x,y,z) = \sum_{n,m} A_{nm} \cos(n\pi x/L) \cos(m\pi y/W) \cosh\{\pi \sqrt{(\rho_c/\rho_{ab})} \sqrt{(n/L)^2 + (m/W)^2} z\} \\ + \sum_{n,m} B_{nm} \cos(n\pi x/L) \cos(m\pi y/W) \sinh\{p \sqrt{(\rho_c/\rho_{ab})} \sqrt{(n/L)^2 + (m/W)^2} z\} + Cz, \quad (10)$$

where n and m are integers ≥ 0 . This solution can be obtained by placing the coordinate origin at the left end corner [refer to Fig. 1(b)]. To have this solution, we also reduce both the current and voltage contact size of the secondary layers from $L/4 \times W$ into $L/4 \times W/4$ in order to simplify the results. Note that in Eq. (10) there are two extra terms, B_{mm} and C , as compared to Eq. (3); these two terms are introduced to meet the boundary condition at the primary and the

secondary layers. By using the double integration on the bottom layer ($z=0$) and assuming $m=n=0$, we have

$$C = \frac{\rho_c I}{LW}. \quad (11)$$

For $m=0$, we find

$$B_{n0} = \frac{8kI \sin(n\pi/4)}{n^2 \pi^2 W}, \quad (12)$$

for $n=0$,

$$B_{0m} = \frac{8kI \sin(m\pi/4)}{m^2 \pi^2 L}, \quad (13)$$

and for n and $m > 0$,

$$B_{nm} = \frac{64kI \sin(n\pi/4) \sin(m\pi/4)}{nmLW\pi^3 \sqrt{(n/L)^2 + (m/W)^2}}. \quad (14)$$

With all the above coefficients and assuming $m=0$, the integration on the primary layer ($z=D$) give

$$A_{n0} = \frac{-8kI \sin(n\pi/4)}{n^2 \pi^2 W} \left(\frac{\cosh(pn\pi D/L) - 1}{\sinh(pn\pi D/L)} \right). \quad (15)$$

Assuming $n=0$, we have

$$A_{0m} = \frac{-8kI \sin(m\pi/4)}{m^2 \pi^2 L} \left(\frac{\cosh(pm\pi D/W) - 1}{\sinh(pm\pi D/W)} \right), \quad (16)$$

and for n and $m > 0$, one finds

$$A_{nm} = \frac{-64kI \sin(m\pi/4) \sin(n\pi/4) \cos(n\pi x/L) \cos(m\pi y/W)}{nm\pi^3 LW \sqrt{(n/L)^2 + (m/W)^2}} \left(\frac{\cosh[p\pi \sqrt{(n/L)^2 + (m/W)^2} D] - 1}{\sinh[p\pi \sqrt{(n/L)^2 + (m/W)^2} D]} \right). \quad (17)$$

Given all the above coefficients, we compute the potential difference between points $(x, y, z=D)$ and $(x, y, z=0)$:

$$\begin{aligned} V_c(x, y) = & \sum_{m=1}^{\infty} \frac{16kI \sin(m\pi/4) \cos(m\pi y/W)}{m^2 \pi^2 L} \left(\frac{\cosh(pm\pi D/W) - 1}{\sinh(pm\pi D/W)} \right) \\ & + \sum_{n=1}^{\infty} \frac{16kI \sin(n\pi/4) \cos(n\pi x/L)}{n^2 \pi^2 W} \left(\frac{\cosh(pn\pi D/L) - 1}{\sinh(pn\pi D/L)} \right) + \frac{\rho_c ID}{LW} \\ & + \sum_{n=1}^{\infty} \sum_{m=1}^{\infty} \frac{128kI \sin(m\pi/4) \sin(n\pi/4) \cos(n\pi x/L) \cos(m\pi y/W)}{nm\pi^3 LW \sqrt{(n/L)^2 + (m/W)^2}} \left(\frac{\cosh[p\pi \sqrt{(n/L)^2 + (m/W)^2} D] - 1}{\sinh[p\pi \sqrt{(n/L)^2 + (m/W)^2} D]} \right). \quad (18) \end{aligned}$$

Once again, we examine the normalized current density as Eq. (19) for the c -axis case on both the primary and secondary layers. With n and m running up to 25, we find that the current density profile agrees with the experimental condition

$$\sum_{m=1}^{\infty} \frac{\sin(m\pi/4) \cos(m\pi y/W)}{2m\pi} + \sum_{n=1}^{\infty} \frac{\sin(n\pi/4) \cos(n\pi x/L)}{2n\pi} + \frac{4 \sin(m\pi/4) \sin(n\pi/4) \cos(n\pi x/L) \cos(m\pi y/W)}{nm\pi^2} + \frac{1}{16}. \quad (19)$$

III. RESULTS AND DISCUSSIONS

We mention that our 3D model is basically equivalent to that of Montgomery, Logan, Rice, and Wick¹² (MLRW). Such equivalence in two dimensions has already been demonstrated by Busch *et al.*¹³ We emphasize, however, that given the tedious processes of rescaling sample dimensions and possibly one having to use an array of image charges¹⁴ to derive the principle resistivities our formulations are much simpler and straightforward. Furthermore our approach is useful to monitor the temperature dependence of the electrical potential profile for given values of resistivities. For instance, in Fig. 2(b) we simulate the electrical potential on the top layer of a crystal near room temperature assuming $\rho_c = 5 \Omega \text{ cm}$ and $\rho_{ab} = 200 \mu\Omega \text{ cm}$. It is found that the potential is quite smooth over the current pads, decreasing rapidly away from the pads.

We examine the applicability of this model to the normal-state voltage data of BSCCO crystals for the derivation of resistivities. We approach this by two means. One simply

uses a pair of voltages V_{ab} and V_c to predict the V_s as shown in Figs. 3(a) and 3(b). For some representative points, we calculate the V_s and find that the theoretical values agree with the data quite well in the normal state with a deviation about $\sim 10\%$ but significant deviation starts to appear toward the transition at about $\sim 88 \text{ K}$ indicating the failure of the model. While the 3 LAR model yields a large peak, on the contrary, the data are rather smooth in that region. The mechanism for the peak is the current leakage from the primary layer to the secondary as illustrated in Eq. (8). This is further supported by the results in Fig. 4(b), where the ρ_c/ρ_{ab} obtained from V_{ab} and V_c clearly decrease more rapidly in transition than that from V_{ab} and V_s . The dissipation seen in V_s will be associated with the quantum coupling of thermal fluctuation which is to be explored in detail later. The seemingly reemergence of the data and the model cannot be taken seriously as we shall demonstrate that in the temperature regime of the secondary peak the system is nonlinear. We also find that the 10% error is irreducible that is presumably due to the simplification of the electrical con-

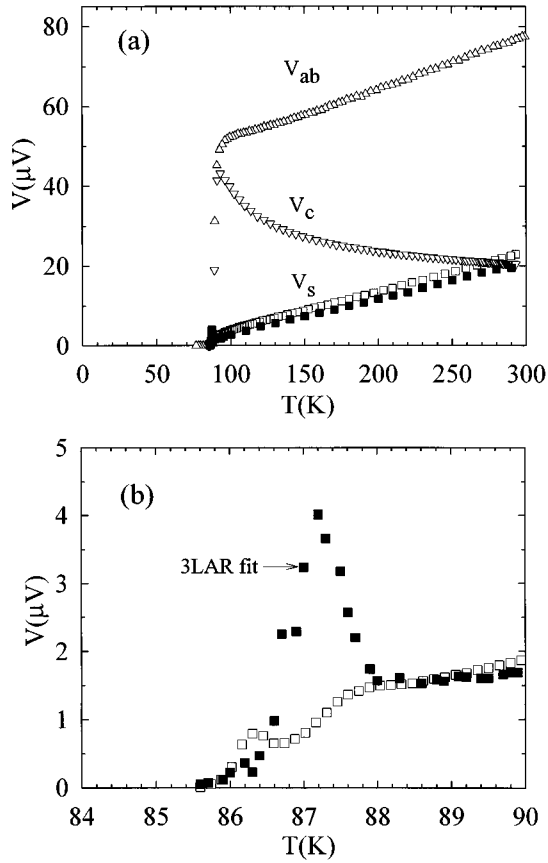


FIG. 3. (a) Normal-state voltage data V_{ab} (Δ), V_s (\square), and V_c (∇) and 3LAR model calculations of V_s (\blacksquare) at a current of 0.1 mA of sample A. (b) Model predictions and V_s data near the transition.

tacts on the secondary layer. In the above calculation, we use Eqs. (7) and (8) to extract $\rho_{ab}(T)$ and $\rho_c(T)$ first, then use the resulting resistivities and Eq. (18) to obtain V_s . The sample parameters are length $L=0.7$ mm, width $W=0.5$ mm, thickness $D=19$ μm , and contact positions are (± 0.35 mm, 0.36 mm, 19 μm) for V_{ab} , (± 0.35 mm, 0 mm, 0 μm) for V_s , and (0.68 mm, 0.05 mm, 19 μm) and (0.68 mm, 0.05 mm, 0 μm) for V_c . By repeating the same calculation using the data of (V_{ab} , V_s), we obtain another set of resistivities. The nearly identical values for the two sets of $\rho_{ab}(T)$ and $\rho_c(T)$ as shown in Fig. 4 are expected. The normal-state anisotropy ratio of $\rho_c(T)/\rho_{ab}(T)$ of the order 10^3 – 10^4 is in good accord with the data reported previously.¹⁵ Although not our main points, the mixture of the metallic feature at $T>150$ K and semimetallic below in the $\rho_c(T)$ as well as the 2–3 times higher values of $\rho_{ab}(T)$ in the normal state are somewhat unexpected that, however, may be associated with either slight sample inhomogeneity¹⁶ or oxygen concentration off the optimum value.¹⁷ The consistency of the model in describing all the data is indisputable indicating the linear nature of the crystals above the transition. To our knowledge, the accuracy of our model analysis is of the best compared to the $\sim 10\%$ of Safar *et al.*¹⁸ and $\sim 50\%$ of Suzuki¹⁹ work in 2D.

Since the electrical transport properties of the BSCCO material cannot be described on the linear basis near the transition [see Figs. 3(b) and 4(b)], in the remainder of this

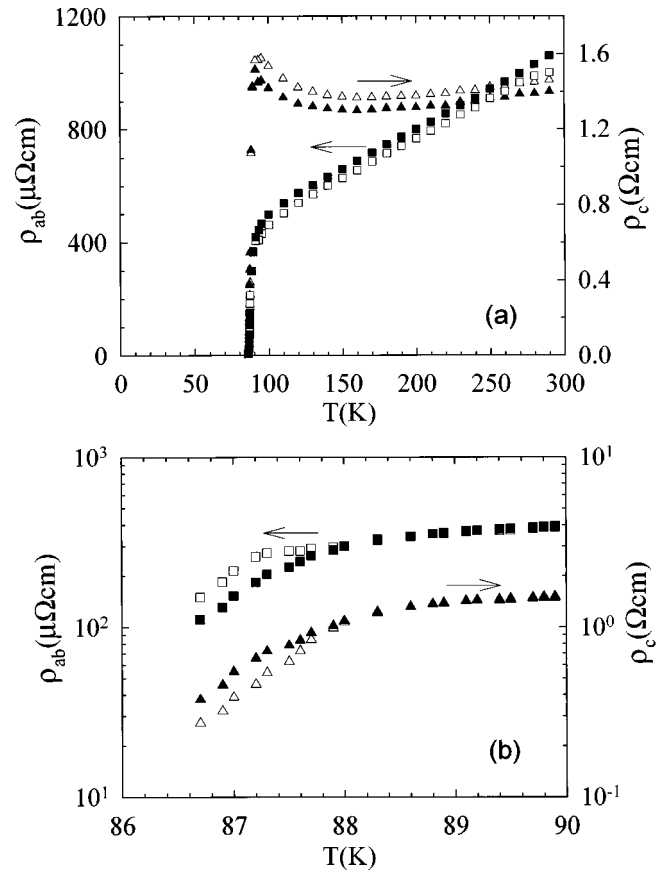


FIG. 4. (a) Normal-state resistivities of sample A derived from the 3LAR model ρ_c (Δ) and ρ_{ab} (\square) are from data V_{ab} and V_c , and ρ_c (\blacktriangle) and ρ_{ab} (\blacksquare) are from V_{ab} and V_s . (b) All the resistivities near the transition.

paper the origin of the nonlinearity and its consequences will be the focus of our discussion. To investigate the crossover from linearity to nonlinearity as the result of the condensation of superfluid in the sample, we examine very carefully the current-voltage characteristics of the ab plane, of the c axis and of the secondary layer by using the dc-flux transformer method. In Fig. 5(a), a family of ab -plane IV curves are presented with a uniform current density on each CuO_2 bilayers of sample B by using four-probe method with current pads on both sides of the sample. Indeed such crossover is observed as the temperature is reduced indicating a 2D type of phase transition. By analyzing the data with the power law $V=I^a(T)$, we find that the exponent $a(T)$ shows a dramatic change from 1 to 3 at ~ 84.8 K as depicted in Fig. 5(b). Such a jump, as predicted by Nelson and Kosterlitz,²⁰ is known to be a consequence of the Lorentz force induced dissociation of thermal vortex pairs, a phenomena well established in 2D superconductors.²¹ Thus we denote 84.8 K as the Kosterlitz-Thouless temperature T_c of this sample. From the linear dependence²² of the $a(T)$ below T_c , which is proportional to the superfluid density, we extrapolate the Ginzberg-Landau mean-field temperature T_{c0} at ~ 86.4 K.

From the IV curves along the c axis [see Fig. 6(a)] of sample C, we find that nonlinearity set in at ~ 86.8 K. Contrary to the ab plane, the mechanism of the nonlinearity is attributed to Josephson tunneling of the superfluid on CuO_2

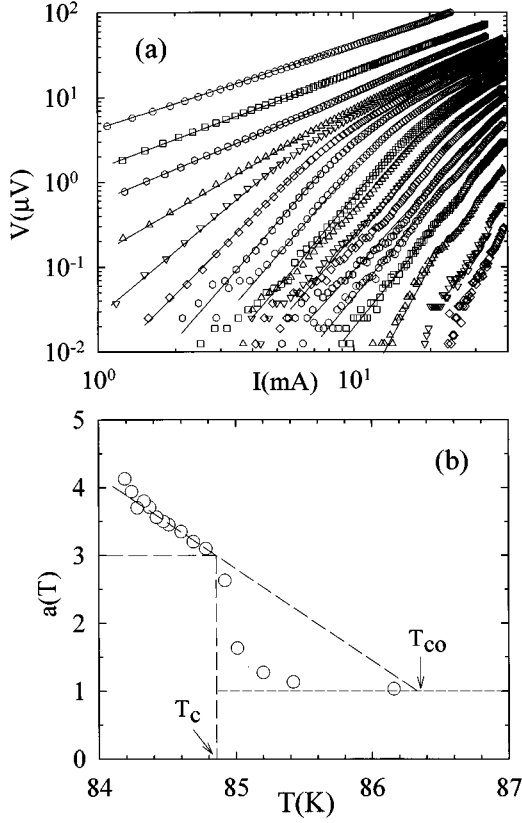


FIG. 5. *Ab*-plane current-voltage characteristics at 86.2, 85.4, 85.2, 85, 84.9, 84.8, 84.7, 84.6, 84.5, 84.47, 84.42, 84.37, 84.33, 84.28, 84.28, 84.19, 84.1, and 84 K of sample *B*. The solid lines are representative fits to the data by using the power law $V = I^{a(T)}$. (b) Temperature dependence of the exponent $a(T)$ with the identified KT temperature T_c and the Ginzberg-Landau mean-field temperature T_{c0} .

bilayers through the insulating BiO layers. Ignoring the non-uniform current effects, the low current behavior may associate with the effects of thermal fluctuations. According to the theory of Ambegaokar and Halperin²³ (AH) for a superconductor-insulator-superconductor (SIS) Josephson tunnel junction, thermal fluctuations could interrupt the phase coherence of superfluid from layer to layer thus introducing detectable dissipation. The equation that describes the current-voltage relation has been derived. Under the circumstance that the bias current does not exceed the critical value, the approximated formulation is

$$V = 2(1-x) \exp \left[-\gamma \left((1-x^2) + \frac{x}{\sin x} \right) \right] \sinh \left(\frac{\pi \gamma x}{2} \right), \quad (20)$$

where $x = I/I_c(T)$, $\gamma = \hbar I_c / eT$, and I_c is the critical current. To compare the theory and the experiment, we plot the theoretical values as solid lines. It is clear that these theoretical results fit the data quite well and provide a sound basis. The fitting parameters of the critical current $I_c(T)$ are obtained and plotted in Fig. 6(b). It is found that the interlayer Josephson current vanishes at about ~ 86.8 K.

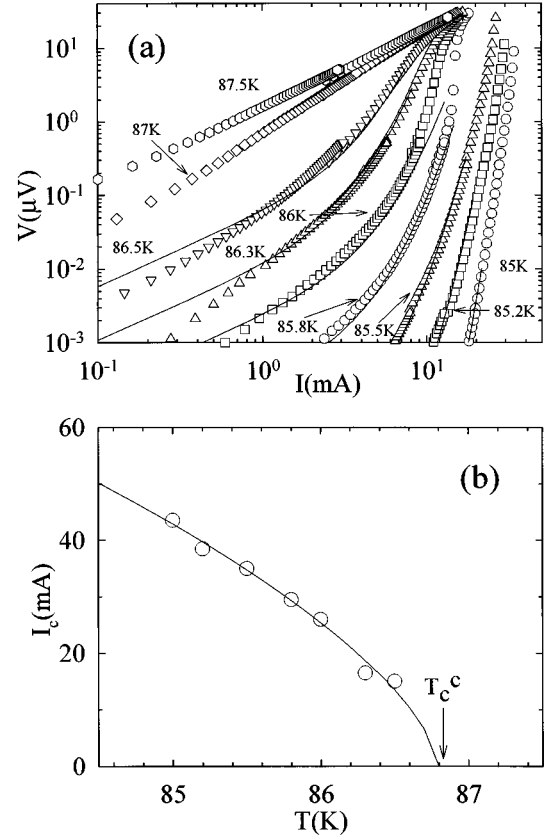


FIG. 6. (a) *c*-axis current-voltage characteristics of sample *C* near transition and model fit. Solid lines are the values from the Ambegaokar-Halperin theory. (b) The temperature dependence of the critical current I_c determined from the theoretical calculations, the solid line is a guide for the eyes.

The *IV* measurements on the same *C* sample of using the dc-flux transformer geometry as shown in Fig. 7(a) yields not only nonlinearity but also with pronounced peaks in the temperature between ~ 86.8 and ~ 84.5 K. These results are analogous to those in Refs. 6 and 24 where the applied current was held at fixed values so we are tempted to use the picture of interlayer coupling to interpret the results. We first note that the peaks appear in the temperature range between the *c*-axis transition temperature $T_c^c \cong 86.8$ K and the *ab*-plane KT temperature $T_c^{ab} \cong 84.5$ K of this sample [see the inset of Fig. 7(b)]. At low current the interlayer coupling strength is stiff and align the 2D vortices from the top to the bottom layers very well so the V_s is linear based on the Bardeen-Stephen flux-flow mechanism.²⁵ At higher currents the V_s increases following power laws due to the dissociation of vortex lines, and finally reaches the critical point that the coupling strength between layers, or the restoring forces, is weakened such that V_s begins to fall off. At the peaks the lateral distance between vortices from a layer to the next one should be larger than the average spacing causing either the effects of vortex cutting,¹³ or vortex melting, or vortex entanglement²⁶ as discussed in other works. Under this guide line, we thus denote the current I_d at the peaks as vortex lines decoupling from 3D to 2D. The temperature dependence of $I_d(T)$ plotted in Fig. 7(b) appears to support this

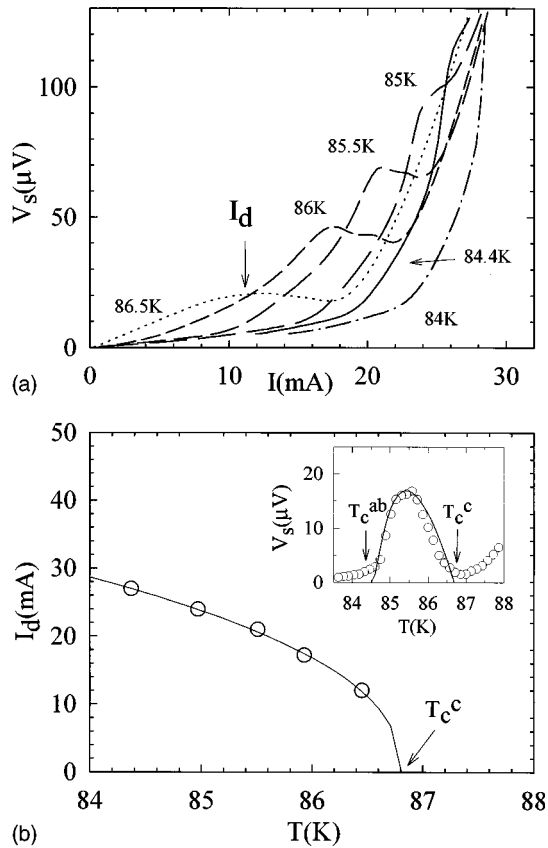


FIG. 7. (a) Current dependence of the secondary voltage $V_s(I)$ near the transition of sample C. I_d is the current for the 3D vortex lines decoupled to 2D. (b) Temperature dependence of I_d , the solid line is a guide line for the eyes. The inset shows V_s at a fixed $I=10$ mA and the determined c -axis and ab -plane transition temperatures by the interlayer vortex coupling model.

interpretation in that the zero I_d temperature is found at ~ 86.8 K which is the temperature where there is no interlayer Josephson interaction. It is interesting to notice that the ~ 2 K temperature window appears to be the effective region for the observation of coupling of thermal vortices. As the

bias current approaching the critical current of the sample, the system becomes linear and the 3LAR model is expected to be effective again.

Lastly we discuss the implications of our results. One of our main conclusions in regard to the origin of the secondary peaks apparently against that of Suzuki who claimed the peaks are due to the leakage of the primary current. This cannot be true since the dependence of the $V_s(I)$ in the current is not linear as would be predicted by the 3LAR model. The interlayer coupling nature of vortices also appears to be valid when magnetic vortices are introduced by an external field. Our experimental results provide another proof for the divergence of the resistivity ratio ρ_c/ρ_{ab} determined from the ab plane and the c -axis measurements by Safar *et al.* although the interpretation for such disparity is in terms of the nonlocal picture.

In summary, we have developed a three-dimensional resistivity model and demonstrated the usefulness of the model to the extreme anisotropic materials of BSCCO 2212 crystals. Our model analysis suggests the ohmic nature of the system above transition and nonlinear below. Measurements of the current-voltage characteristics on the secondary layer confirms the presence of 3D thermal vortex lines. These vortex lines dissociating into weakly interacting 2D vortices is under the influence of a strong applied current in agreement with our earlier work. Thermal fluctuations and the layer nature have been demonstrated to be the key ingredients for these unusual nonlinear phenomena in transition.

ACKNOWLEDGMENTS

We are indebted to Professor W. Saam, Dr. Chris Keener at Ohio State University for many helpful discussions and much assistant from Dr. Y. B. You at National Tsing Hua University. Research at Ohio State University was supported by DOE (MISCON) through Contract No. DE-FG02-90ER45427 and by NSF Grant No. DMR 92-00122 and at Tsing Hua University by NSC of ROC under Contract No. NSC85-2112-M007-043 and -044PH.

- ¹J. M. Kosterlitz and D. J. Thouless, *J. Phys. C* **6**, 1181 (1973).
- ²S. Martin, A. T. Fiory, R. M. Fleming, G. P. Espinosa, and A. S. Cooper, *Phys. Rev. Lett.* **62**, 677 (1989).
- ³S. N. Artemenko, I. G. Gorlova, and Yu. I. Latyshev, *Phys. Lett. A* **138**, 428 (1989).
- ⁴R. Kleiner, F. Steinmeyer, G. Kunkel, and P. Müller, *Phys. Rev. Lett.* **68**, 2394 (1992).
- ⁵L. N. Bulaevskii, M. Ledvij, and V. G. Kogan, *Phys. Rev. Lett.* **68**, 3773 (1992).
- ⁶Y. M. Wan, S. E. Hebboul, D. C. Harris, and J. C. Garland, *Phys. Rev. Lett.* **71**, 157 (1993).
- ⁷T. S. Lee, N. Misert, L. T. Sagdahl, J. Clarke, J. R. Clem, K. Char, J. N. Eckstein, D. K. Fork, L. Lombardo, A. Kapitulnik, L. F. Schneemeyer, J. V. Waszczak, and R. B. van Dover, *Phys. Rev. Lett.* **74**, 2796 (1995).
- ⁸B. Horovitz, *Phys. Rev. Lett.* **72**, 1569 (1994).
- ⁹S. W. Pierson, *Phys. Rev. Lett.* **74**, 2359 (1995).
- ¹⁰Wenbin Yu and D. Stroud, *Phys. Rev. B* **51**, 3725 (1995).
- ¹¹K. K. Uprety and D. Domínguez, *Phys. Rev. B* **51**, 5955 (1995).
- ¹²H. C. Montgomery, *J. Appl. Phys.* **42**, 2971 (1971); B. F. Logan, S. O. Rice, and R. F. Wick, *ibid.* **42**, 2975 (1971).
- ¹³R. Busch, G. Ries, H. Werthner, G. Kreiselmeyer, and G. Saemann-Isschenko, *Phys. Rev. Lett.* **69**, 522 (1992).
- ¹⁴S. Martin, A. T. Fiory, R. M. Fleming, L. F. Schneemeyer, and J. V. Waszczak, *Phys. Rev. Lett.* **60**, 2194 (1988).
- ¹⁵G. Briceño, M. F. Crommie, and A. Zettl, *Phys. Rev. Lett.* **66**, 2164 (1991).
- ¹⁶R. Jin, H. R. Ott, and D. P. Grindatto, *Physica C* **250**, 395 (1995).
- ¹⁷T. Yasuda, S. Takano, and L. Rinderer, *Physica C* **208**, 385 (1993).
- ¹⁸H. Safar, P. L. Gammel, D. A. Huse, S. N. Majumdar, L. F. Schneemeyer, D. A. Bishop, D. López, G. Nieva, and F. de la Cruz, *Phys. Rev. Lett.* **72**, 1272 (1994).
- ¹⁹M. Suzuki, *Phys. Rev. B* **50**, 6360 (1994).
- ²⁰D. R. Nelson and J. M. Kosterlitz, *Phys. Rev. Lett.* **39**, 1201 (1977).

- ²¹J. C. Garland and Hu Jong Lee, Phys. Rev. B **36**, 3638 (1987), and references therein.
- ²²A. M. Kadin, K. Epstein, and A. M. Goldman, Phys. Rev. B **27**, 6691 (1983).
- ²³V. Ambegaokar and B. I. Halperin, Phys. Rev. Lett. **22**, 1364 (1969).
- ²⁴Y. M. Wan, S. E. Hebboul, and J. C. Garland, Phys. Rev. Lett. **72**, 3867 (1994).
- ²⁵J. Bardeen and M. J. Stephen, Phys. Rev. **140**, A1197 (1965).
- ²⁶D. R. Nelson, Phys. Rev. Lett. **60**, 1973 (1988).